Helmholtz-Zentrum Dresden-Rossendorf (HZDR)

High-field soft-x-ray dichroism of a hard ferrimagnet with easy-plane anisotropy

Yamamoto, S.; Gorbunov, D.; Diaz-Ortega, I. F.; Miyata, A.; Kihara, T.; Kotani, Y.; Nakamura, T.; Mushnikov, N. V.; Andreev, A. V.; Nojiri, H.; Wosnitza, J.;

High-field soft-x-ray dichroism of a hard ferrimagnet with easy-plane anisotropy

Sh. Yamamoto,[1, *] D. I. Gorbunov,[1] I. F. Diaz-Ortega,[2] A. Miyata,[1] T. Kihara,[2] Y. Kotani,[3]
T. Nakamura,[2, 3] N. V. Mushnikov,[4] A. V. Andreev,[5] H. Nojiri,[2] and J. Wosnitza[1, 6]

[1]*Hochfeld-Magnetlabor Dresden (HLD-EMFL) and Würzburg-Dresden Cluster of Excellence ct.qmat,
Helmholtz-Zentrum Dresden-Rossendorf, 01328 Dresden, Germany*
[2]*Institute for Materials Research, Tohoku University, Sendai 980-8577, Japan*
[3]*Japan Synchrotron Radiation Research Institute, SPring-8, Sayo, Hyogo 679-5198, Japan*
[4]*Institute of Metal Physics, Ural Branch of the Russian Academy of Sciences,
Kovalevskaya 18, 620990 Ekaterinburg, Russia*
[5]*FZU Institute of Physics, Czech Academy of Sciences, 18221 Prague, Czech Republic*
[6]*Institut für Festkörper- und Materialphysik, TU Dresden, 01062 Dresden, Germany*
(Dated: July 30, 2021)

We performed soft x-ray spectroscopic studies of the ferrimagnet $TbFe_5Al_7$ with strong easy-plane anisotropy in pulsed magnetic fields up to 29 T along with bulk magnetization and magnetostriction measurements. We observed pronounced amplitude changes of x-ray magnetic circular dichroism and x-ray absorption spectra at the field-induced magnetic transition. This microscopically evidences the simultaneous rotation of the Tb $4f$ and Fe $3d$ magnetic moments from a collinear ferrimagnetic order along the [100] axis to a state with the moments close to [010], the other easy-axis direction of the tetragonal lattice in magnetic fields applied along the [100] axis. We determined the magnetic-anisotropy constant of $TbFe_5Al_7$ by simulating the high-field macro- and microscopic magnetization process using a two-sublattice model.

I. INTRODUCTION

The intriguing magnetic properties of rare-earth (R) transition-metal (T) intermetallic compounds continue to attract a lot of attention. This material class forms one of the most fundamental components in a variety of applications such as permanent magnets, magnetostrictive, magneto-optic, spintronic, and magnetic-refrigeration devices [1]. The good hard magnetic properties originate from the individual R and T sublattices that are coupled through a $3d$-$4f$ intersublattice interaction. This coupling transfers the large magnetic anisotropy of the R to the T sublattice and the strong exchange interactions of the T to the R sublattice [2].

The magnetic coupling between the $3d$ and $4f$ moments is antiparallel for R-T compounds with magnetic heavy R elements. This antiparallel arrangement leads to a ferrimagnetic order that can be broken by a sufficiently strong applied magnetic field, typically tens to hundreds of tesla, comparable to the strength of the R-T coupling [3]. The breaking of the initial ferrimagnetic alignment usually manifests as magnetization jumps in the presence of anisotropy [4–9]. Conventional high-field bulk magnetization experiments measure only the total macroscopic moment composed of R and T sublattices [10]. However, for a thorough understanding and modeling of field-induced phase transitions, it is important to elucidate the magnetization process of the magnetic atoms individually. Especially, hard $R - T$ magnets exhibit large field-induced noncollinearity [11]. The investigation of element-specific magnetic properties enable to extract quantitative information on the exchange interactions and magnetocrystalline anisotropy.

The highly anisotropic ferrimagnets RFe_5Al_7 (R = Tb, Dy, Ho, Er, and Tm) show field-induced magnetic transitions as applied magnetic fields tune the exchange and anisotropy interactions [12]. These materials crystallizes in the tetragonal crystal structure of $ThMn_{12}$ type (space group $I4/mmm$) [13]. There are two types of magnetic anisotropies in RFe_5Al_7: easy-plane anisotropy for R = Tb, Dy, Ho, and Er and easy-axis anisotropy for R = Tm [12]. The anisotropic character dominantly comes from the single-ion nature in the R $4f$ sublattice, while the Fe sublattice displays easy-plane anisotropy [14]. In the model of single-ion aniosotropy, the type of the magnetic anisotropy follows the sign of the second-order Stevens' factor α_J in first approximation. For the easy-axis system $TmFe_5Al_7$, the sign of α_J is positive. On the other hand, for the easy-plane system, the sign of α_J is negative except for R = Er. In $ErFe_5Al_7$, higher-order Stevens' factors most likely dominantly provide the negative contribution to the anisotropy of the Er sublattice [15]. Among the heavy R elements with negative α_J, the Tb^{3+} ion has the largest α_J and $TbFe_5Al_7$ shows the highest magnetic anisotropy in the RFe_5Al_7 family [16].

In the easy-axis system (R = Tm), recent high-field soft x-ray magnetic circular dichroism (XMCD) experiments revealed that the field-induced magnetic transitions correspond to the simultaneous moment rotation from a ferrimagnetic to a canted state close to a forced ferromagnetic state [17, 18]. The magnetic anisotropy reflecting the local magnetic symmetry plays a crucial role in the high-field magnetic properties. Therefore, the field-induced magnetic transition in the easy-plane systems is expected to be different from that in the easy-axis system. High-field Fe K-edge XMCD measurements of the easy-plane system $HoFe_5Al_7$ indeed are in line with such a scenario [19]. However, the Fe K-edge XMCD, in general, contains

both R and T contributions due to the magnetic coupling via the R $5d$ electrons in R-T intermetallic compounds [20, 21]. This makes it challenging to obtain element- and shell-selective magnetic properties. On the other hand, the R $4f$ and T $3d$ shells can be directly accessed via electric-dipole transitions in the soft x-ray range. In the present study, we investigate the element-selective magnetic properties in the easy-plane system TbFe$_5$Al$_7$ at high magnetic fields.

TbFe$_5$Al$_7$ exhibits ferrimagnetic order below the Curie temperature of 242 K [22]. A strong anisotropy is also present in the basal plane of the tetragonal lattice. With increasing temperature, the easy-magnetization direction changes from the [100] to the [110] axis via a spontaneous spin reorientation in the vicinity of the magnetic compensation point, $T_{\mathrm{comp}} = 84$ K. The competition between intra- and inter-sublattice exchange interactions with each other and with the crystal electric field could bring about phase transitions in applied magnetic field as the initial collinear ferrimagnetic structure first transforms into a canted structure and finally into a forced ferromagnetic state. However, TbFe$_5$Al$_7$ shows a small, almost negligible anomaly in the magnetization for field applied along the easy [100] direction at 2 K [16]. This anomaly develops into a pronounced field-induced phase transition at elevated temperatures. This unexpected finding calls for additional effort to understand the low-temperature magnetic properties of TbFe$_5$Al$_7$.

TbFe$_5$Al$_7$ adopts an amplitude-modulated magnetic structure at low temperatures where a weak field-induced phase transition is observed [28]. Here, by performing time-dependent magnetization measurements, we show a possible crossover close to 40 K to a state where a pronounced field-induced transition takes place. Using advanced soft x-ray spectroscopy in pulsed magnetic fields in combination with magnetization measurements, we show that unlike the easy-axis system ($R = $ Tm), the easy-plane system ($R = $ Tb) shows a moment rotation at the field-induced transition from the collinear ferrimagnet to a state with sublattice moments close to the other easy-axis direction within the basal plane. This reflects different magnetic symmetries between the two cases. Our macro- and microscopic magnetization data were simulated using a two-sublattice model, which enabled us to extract a fundamental magnetic parameter, i.e., the in-plane anisotropy constant. We further employed magnetostriction measurements to clarify the role of the lattice degrees of freedom at the field-induced phase transitions. This was motivated by our earlier observation of large anomalies in sound velocity that suggest strong spin-lattice coupling in TbFe$_5$Al$_7$ [16].

II. EXPERIMENTAL DETAILS

Magnetization measurements at constant temperature as a function of time were performed using a standard PPMS magnetometer. High-field magnetization and longitudinal magnetostriction measurements were performed using a coaxial pickup-coil system [23] and an optical fiber Bragg-grating technique [24], respectively. High-field soft x-ray spectroscopy experiments were conducted at the twin-helical undulator beamline BL25SU [25] at SPring-8. The degree of circular polarization in the current experiment was 96 % [26]. Absorption signals were detected in the total-electron yield (TEY) mode. The sample was *in situ* cleaved parallel to the (100) plane, which is normal to the x-ray propagation direction, at pressures below 2×10^{-7} Pa to obtain a clean surface. The averaged x-ray absorption spectrum (XAS) and XMCD spectra were obtained from $(\mu_+ + \mu_-)/2$ and $\mu_+ \text{-} \mu_-$, where μ_+ (μ_-) is the TEY signal measured with plus (minus) helicity. Fields up to 29 T were generated using a pulsed magnet with a capacitor charging voltage of 2 kV. Experimental details regarding the pulsed-field soft x-ray spectroscopy are described elsewhere [17, 27]. The soft x-ray measurements were performed below 50 K for field applied along the [100] axis.

III. RESULTS AND DISCUSSION

Figures 1(a) and 1(b) show XMCD spectra at 20 K at the Tb M_5 and Fe L_3 edge, respectively, after the applied field was removed, which signals antiparallel coupling between the Tb $4f$ and Fe $3d$ moments along the [100] axis. We measured the field-dependent XMCD amplitudes using photon energies, at which we observed maximum XMCD in pulsed-magnetic fields at selected temperatures [Figs. 1(c) and 1(d)]. With decreasing temperature, the overall XMCD signal at both absorption edges decreases.

TbFe$_5$Al$_7$ shows an amplitude-modulated magnetic structure at low temperatures [28]. This is in line with the large magnetic anisotropy contributed by the Tb sublattice. The anisotropy forces the magnetic moments to align along the easy [100] axis but their amplitudes are modulated (for a weak anisotropy, helimagnetic structures are usually observed [29]). Our XMCD data seem to confirm this picture: The Tb and Fe magnetic moments reduce with decreasing temperature [Figs. 1(c) and 1(d)]. Additionally, diffuse scattering was reported for TbFe$_5$Al$_7$, which is associated with a short-range ferrimagnetic order at low temperatures [28]. This is also in line with the reduced Tb and Fe magnetic moments.

The amplitude-modulated structure changes to a non-modulated structure at elevated temperatures [28]. However, no anomalies were observed in the temperature dependences of the specific heat, magnetization, and elastic properties except at the spin-reorientation temperature at 84 K [16, 22]. This suggests that either the transition is weak with a small release of magnetic entropy or the magnetic structure becomes non-modulated at the same temperature as the spin reorientation. In a neutron-diffraction experiment, the satellite reflections that evidence the
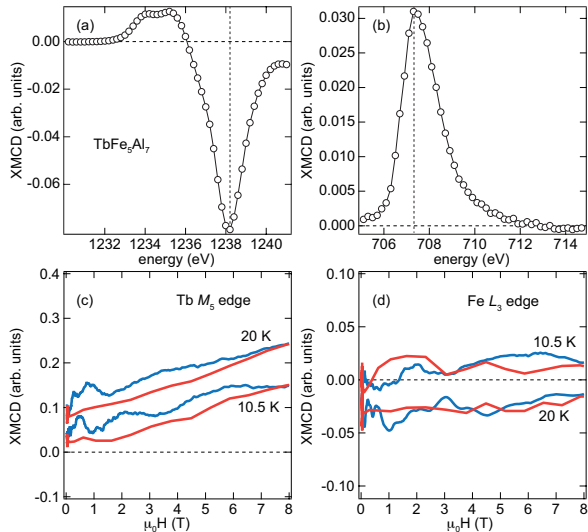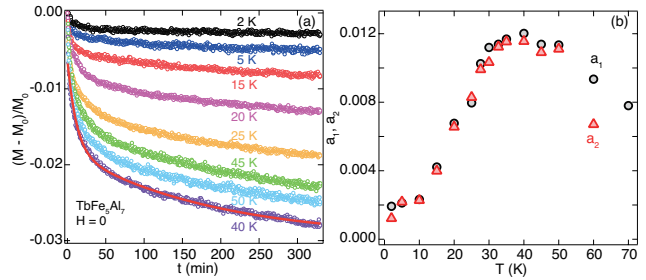
FIG. 2: (a) Time dependence of remnant magnetization (symbols) at selected temperatures after removing the cooling magnetic field of 14 T. The solid line is the fit of the double exponential function to the time evolution of magnetization at 40 K. (b) Relative amplitude of each exponential component, defined by Eq. (1), as a function of temperature.

FIG. 1: XMCD spectra at the (a) Tb M_5 and (b) Fe L_3 edge. These spectra were obtained in zero field at 20 K after a field pulse of 10 T was applied along the [100] axis. The vertical dashed lines represent the photon energies at which magnetic-field-dependent XMCD data of (c) Tb and (d) Fe at 20 K and 10.5 K were recorded. The spectra are normalized to the XAS intensity at each energy and temperature. The sign of the XMCD in (c) and (d) is reversed with respect to those in (a) and (b). The positive (negative) values of the reversed Tb M_5- and Fe L_3-edge XMCD signals correspond to the moment direction (anti)parallel to the field direction.

modulation disappear around 100 K [28].

Earlier magnetization measurements of $TbFe_5Al_7$ showed displaced non-symmetric hysteresis loops below 40 K for field applied along the easy [100] axis [22]. We checked the hypothesis of a spin-glass state, put forward in Ref. [30], and found no evidence for such a state from frequency dependent magnetic-susceptibility measurements (not shown). We also performed time-dependent magnetization measurements. First, the sample was cooled down from room temperature to the target temperature in 14 T. Then, the field was removed and the magnetization was measured at a constant temperature as a function of time. We found a substantial relaxation over several hours [Fig. 2(a)]. The normalized magnetization, $(M - M_0)/M_0$, where M_0 is the magnetization at time $t = 0$, shows the largest effect, ~ 2.5 %, at 40 K. We could describe the experimental data using a sum of two exponential functions,

$$\frac{M(t) - M_0}{M_0} = a_1 \exp\left(-\frac{t}{\tau_1}\right) + a_2 \exp\left(-\frac{t}{\tau_2}\right) + b,$$
(1)

where a_1 and a_2 are coefficients, τ_1 and τ_2 are relaxation times, and b is an offset. We obtained $\tau_1 \approx 500$ sec and $\tau_2 \approx 12000$ sec between 2 and 70 K, whereas a_1 and a_2 show a maximum at around 40 K [Fig. 2(b)]. Thus, $TbFe_5Al_7$ seems to show two distinct magnetic states with a possible crossover close

to 40 K. This result corresponds well to the temperature range where the non-symmetric hysteresis loops are no longer observed, ~ 40 K [22], and where a pronounced field-induced phase transition develops, ~ 50 K [16], for field applied along the easy [100] axis [Figs. 3(a) and 3(b)]. Additional microscopic measurements are required to determine the nature of the low-temperature state of $TbFe_5Al_7$.

Figure 3(a) shows the field dependence of the magnetization at 50 K. The magnetization curve was recorded after applying a negative magnetic-field pulse, which results in a negative remanence as the initial state. This was taken by offsetting the pulsed-field data according to static-field magnetization results performed on the same sample. Two regions with hysteresis appeared between 0 – 8 T and 12 – 20 T. The former presumably reflects domain-wall motion [22], while the latter corresponds to the field-induced first-order magnetic transition. Above 20 T, magnetization monotonously increases and does not reach magnetic saturation up to 60 T [16].

Figure 3(b) shows the field dependence of the relative length change, $\Delta L/L$, along the field direction. Initially, the sample is in a multi-domain state that consists of two types of domains with the magnetic moments aligned along the easy [100] direction. Application of field forces domain-wall motion, which changes only one type of domains with a total magnetization antiparallel to the field direction. The domain-wall motion leads to a positive linear magnetostriction of 2×10^{-4}. As the field increases further, it induces a spin reorientation near 20 T from one easy magnetization direction, [100], to the other, [010], within the basal plane (see below). This spin reorientation is accompanied by a negative linear magnetostriction, $\sim 4 \times 10^{-4}$. This effect is twice as large as compared to that due to the domain-wall motion since twice as many domains change their orientation at the field-induced transition.

Figure 3(c) shows the transition field of the first-order transition in Figs. 3(a) and 3(b) as a function of temperature. The phase boundary is drawn by a gray
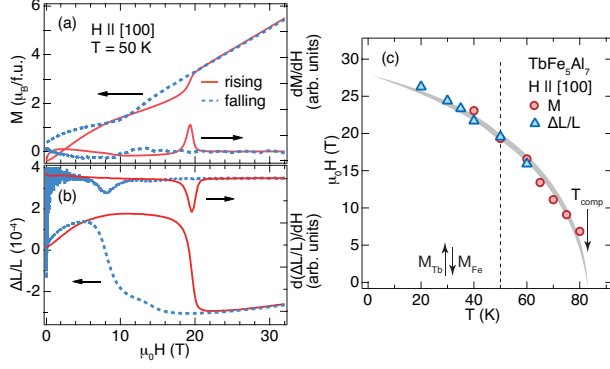
FIG. 3: (a) Magnetization and (b) longitudinal magne-
tostriction $\Delta L/L$ (left scale) and its field derivative (right
scale) at 50 K as function of magnetic field applied along
the [100] axis. (c) H-T phase diagram of TbFe$_5$Al$_7$ with
magnetic field applied along the [100] axis determined by
peak positions in dM/dH and d($\Delta L/L$)/dH data taken
during field upsweep. The gray solid line is a guide for the
eyes. Soft x-ray spectra in pulsed magnetic fields, shown
in Figs. 4, 5, and 6, were measured along the dashed
vertical line. The antiparallel arrows sketch the collinear
ferrimagnetic structure below T_{comp}.

FIG. 4: (a) Tb M-edge and (b) Fe L-edge XMCD spectra
at selected magnetic fields during the up sweep in pulsed
magnetic fields at 50 K. All spectra are normalized to the
(a) M-edge and (b) L-edge XAS integral at each field.

line deduced from magnetization and longitudinal-
magnetostriction anomalies. Above T_{comp}, we did
not observe field-induced transitions along the [100]
axis. Field-induced transitions were observed along
the easy [110] axis by magnetization and acoustic
measurements above T_{comp} [16].

Now, we present the results of high-field soft x-ray
spectroscopy at 50 K. Figures 4(a) and 4(b) show Tb
M-edge ($3d \rightarrow 4f$) and Fe L-edge ($2p \rightarrow 3d$) XMCD
spectra at selected magnetic fields measured during
the upsweep of pulsed magnetic fields, respectively.
The Tb M and Fe L-edge spectra at 10 T are in good
agreement with those observed in previous studies for
Tb^{3+} [31] and metallic Fe [32]. Figure 4 shows dif-
ferent signs of the XMCD signals for Tb M_5 and Fe
L_3 at 10 T, which evidences the antiferromagnetic
coupling between the two sublattices, with the Tb $4f$
(Fe $3d$) magnetic moment (anti)parallel to the field
direction.

Below 10 T, the XMCD spectral lineshapes at both
Tb M and Fe L edges remain unchanged. The XMCD
signals exhibit a slight reduction in magnitude at
both edges with increasing fields up to 10 T. Close
to the critical field around 19 – 20 T (Fig. 3), we
observed drastic changes of the XMCD signal ampli-
tude, which reflect the step-wise changes of the Tb
$4f$ and Fe $3d$ magnetic moments along the [100] axis.
With increasing fields, the Tb XMCD spectral ampli-
tude markedly decreases above 17 T, reaches a min-
imum at 23 T, and then increases slightly up to 28
T [Fig. 2(a)]. The Fe XMCD signal decreases as
well above 17 T, and becomes zero at 21.5 T. Then,
the XMCD amplitude grows up to 28 T with oppo-
site sign with respect to that at lower fields. The
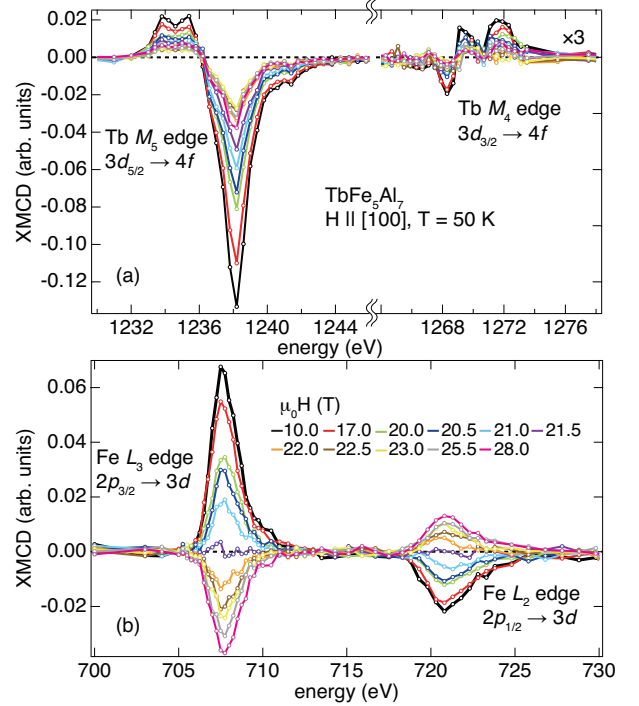spectral lineshapes of both edges do not display any

changes, which means that the local ligand environ-
ments do not affect the XMCD spectra in the current
field range. Therefore, the amplitude variations of the
XMCD spectra are directly related to the changes of
Tb and Fe sublattice moments.

The lineshape of the averaged XAS [$= (\mu_+ + \mu_-)/2$]
at the Tb M edge depends on the magnetic field. Fig-
ure 5(a) compares the Tb XAS at 10 T and 28 T. At
the Tb M_5 edge, the XAS at 28 T has a main peak
at a lower photon energy than that at 10 T, while
at the M_4 edge, the whole XAS amplitude at 28 T is
larger than that at 10 T. In order to obtain further in-
sights into the modification of the XAS lineshape in
magnetic fields, XAS difference spectra, defined by
XAS(H)-XAS(0 T), at selected magnetic fields are
shown in Fig. 5(b), where XAS(H) and XAS(0 T)
represent the XAS obtained at a certain magnetic
field H and at zero field, respectively. The XAS dif-
ference spectrum at 10 T is almost zero in the whole
Tb M-edge energy region. However, with increasing
the field from 17 to 23 T, positive and negative peaks
appear with increasing photon energy at the M_5 edge
and a positive peak at the M_4 edge. This pronounced
changes in the averaged XAS and its difference spec-
tra occur near the field-induced magnetic transition
(Fig. 3). At 10 T, the Tb $4f$ moment points along the
[100] direction and perpendicular to the plane of the
electric-field (E) vector of the incident beam [inset of
Fig. 5(a)]. On the other hand, at 28 T the longitudi-
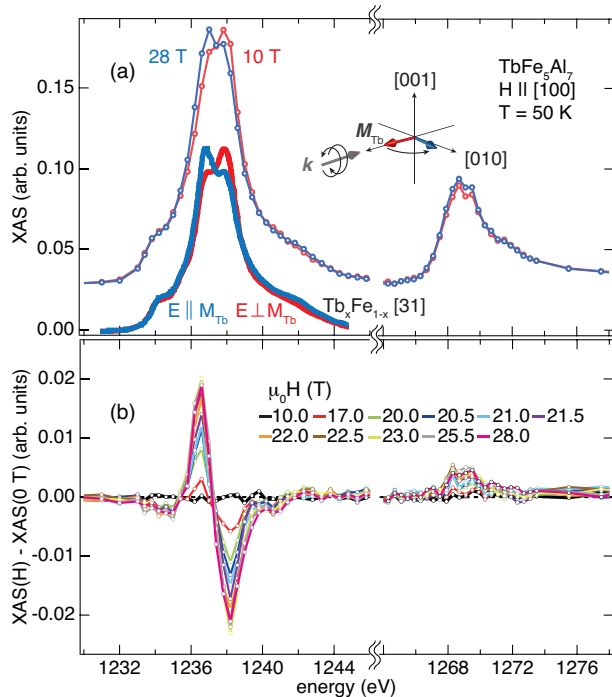nal Tb $4f$ moment is reduced when compared to that

FIG. 5: (a) Averaged Tb M-edge XAS spectra at 10 T (red) and 28 T (blue) compared with Tb M_5-edge XAS spectra measured by using linear polarization perpendicular (red) and close to parallel (blue) to the Tb moments of $Tb_x Fe_{1-x}$ [34]. The inset shows the Tb $4f$-moment direction in the (001) plane, M_{Tb}, at 10 T (red arrow) and 28 T (blue arrow) with respect to the beam propagation direction, k (see text for details). (b) XAS spectra at 0 T [XAS(0T)] subtracted from the XAS spectra at selected magnetic fields [XAS(H)] obtained during field upsweep.

at 10 T as observed in Fig. 4(a).

The variations in the averaged XAS and its difference spectra can be regarded as the response to the x-ray magnetic linear dichroism (XMLD) effect based on the following facts: 1) The sum of the left and right circularly polarized light, in principle, corresponds to the linear polarization, 2) the averaged XAS lineshapes at 10 T and 28 T match those of previously reported Tb M-edge XAS spectra with linear polarization oriented perpendicular and parallel to the Tb $4f$ moment [Fig. 5(a)] [33, 34], respectively, and 3) the XAS difference spectra [Fig. 5(b)] also agree with the Tb M-edge XMLD spectra in the earlier studies. Therefore, in high magnetic fields at the magnetic transition, transverse components of the Tb $4f$ moment emerge, which are perpendicular to the beam direction [inset of Fig. 5(a)]. We note that further experiments on high-field XMLD spectroscopy using linear polarization could provide information on the Tb moment orientation within the (100) plane. In comparison to the XAS difference at the Tb M edge, the finite magnitudes of the Fe L-edge XAS difference were not detected within the current experimental resolution of the pulsed-field setup. This is related to the fact that XMLD effects in T $3d$ systems are

extremely small due to much smaller spin-orbit interaction in the T $3d$ than in the R $4f$ shell [35, 36].

Since the XMCD lineshapes at the Tb M and Fe L edges do not display observable field-dependent variations, the changes in the XMCD intensity directly reflect the modifications of the respective sublattice moment along the beam-propagation direction. One observes simultaneous rotations of the Tb and Fe magnetic moments at the field-induced transition (Fig. 6). Figure 6(a) shows the field dependence of the integrated XMCD signal at the Tb M_5 and Fe L_3 edges. When the longitudinal component of the Fe $3d$ moment reverses at the field-induced first-order magnetic transition at about 20 T (Fig. 3), the longitudinal Tb $4f$ moment strongly reduces. Above the field-induced transition, both Tb and Fe moments along the [100] axis gradually increase up to the highest magnetic field.

Figure 6(b) shows the integrated magnitude of the negative peak in the XAS difference spectra at the Tb M_5 edge [Fig. 5(b)] as function of magnetic field, which reflects the transverse Tb $4f$ moment. This also shows hysteretic behavior at the magnetic transition. The finite transverse Tb moment appears when the Tb XMCD integral, or longitudinal component, starts to decrease. After reaching a maximum near 23 T, the transverse component slightly decreases. In some cases, a field-induced ferri-to-ferromagnetic transition was suggested to occur through a continuous magnetization change, which involves with only longitudinal variations [7]. However, the current study microscopically evidences that the field-induced phase transitions in $TbFe_5Al_7$ take place through sublattice-moment rotations.

The element-selective moment rotation in magnetic fields is schematically shown in Fig. 6(d) extracted from Fig. 6(a) by assuming that the XMCD amplitudes correspond to the projected moment along the [100] direction. Due to the antiferromagnetic coupling between the Tb $4f$ and Fe $3d$ moment, the Fe $3d$ moment rotates along with the rotation of the Tb $4f$ moment. In our previous work using hard x-rays [19], we suggested that the field-induced magnetic transition in $HoFe_5Al_7$, a system with easy-plane anisotropy, originates in the moment rotation from one easy-axis direction to another one in the basal plane of the tetragonal lattice. This is evidenced directly in the current study, where the sublattice Tb $4f$ and Fe $3d$ moments rotate from [100] to a direction close to the [010] axis [Fig. 6(d)] at the field-induced transition. This is in contrast to $TmFe_5Al_7$ with easy-axis anisotropy, for which the field-induced magnetic transition is linked to a stepwise rotation from the ferrimagnetic order to the state close to the forced ferromagnetic state [17]. Contrary to $TbFe_5Al_7$, $TmFe_5Al_7$ does not have any equivalent direction to the [001] axis during the moment rotation. This different magnetic-symmetry properties between RFe_5Al_7 with the easy-plane ($R = $ Tb) and easy-axis ($R = $ Tm) anisotropy leads to the different rotation schemes directly observed by the soft x-ray techniques.
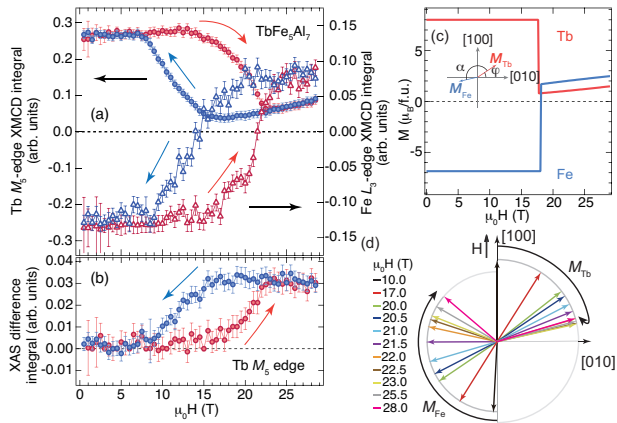
FIG. 6: Field dependence of (a) the integrated Tb M_5-edge (left) and Fe L_3-edge (right) XMCD signal and (b) the integrated Tb M_5-edge XAS difference at 50 K. The sign of the integrated XMCD signal in panel (a) is reversed as in Figs. 1(c) and (d). (c) Tb $4f$ (M_{Tb}) and Fe $3d$ (M_{Fe}) moment as function of magnetic field simulated by the two-sublattice model. The inset shows the canting angles used in the simulation (see text for details). (d) Schematic diagram of the sublattice-moment rotation in magnetic field estimated from the data in (a) and (b) during the field upsweep. The black arrows show the rotation direction on increasing magnetic fields.

Our microscopic data make it possible to model the magnetization process of the individual Tb and Fe sublattices at 50 K. To this end, we considered the following free-energy expansion:

$$
\begin{aligned}
E(\alpha, \varphi, H) = {} & M_{\mathrm{Tb}} M_{\mathrm{Fe}} n_{\mathrm{TbFe}} \cos(\alpha) - K \cos(4\varphi) \\
& - \mu_0 H [M_{\mathrm{Tb}} \sin(\varphi) + M_{\mathrm{Fe}} \sin(\varphi + \alpha)],
\end{aligned}
\tag{2}
$$

where the first, second, and third term are the inter-sublattice exchange energy, anisotropy energy within the basal plane, and Zeeman energy, respectively. M_{Tb} and M_{Fe} are the Tb and Fe sublattice moments, respectively, $n_{\mathrm{TbFe}} = 6.8$ T f.u./μ_{B} is the intersublattice exchange constant [16], K is the in-plane anisotropy constant both from the Tb and Fe sublattices, φ is the angle between the Tb moment and the [010] axis, α is the angle between the Tb and Fe moments [inset of Fig. 6(c)].

We minimized the free energy with respect to the angles α and φ. Using the obtained α and φ values, we calculated the magnetization of the individual Tb and Fe sublattices as a function of applied field [Fig.

6(c)]. The only fit parameter was K. The calculations show a good qualitative agreement with the experiment by reproducing the step-wise rotations of the Tb and Fe magnetic moments between 18 and 19 T. The best fit to the experimental data yielded $K \simeq 1$ MJ/m^3 at 50 K. This value is larger than that found for HoFe$_5$Al$_7$ at 11 K, 0.5 MJ/m^3 [19], which is due to the larger contribution of Tb to the magnetocrystalline anisotropy.

IV. CONCLUSION

In summary, our element-selective soft x-ray magnetic dichroism measurements in high magnetic fields reveal the individual magnetic response of Tb $4f$ and Fe $3d$ moments in the highly anisotropic easy-plane ferrimagnet TbFe$_5$Al$_7$. At the field-induced magnetic transition, both magnetic moments rotate simultaneously within the basal plane of the tetragonal lattice. Starting from the initial collinear ferrimagnetic order, with alignment along the [100] axis, the moments rotate to the other easy axis within the plane, namely along [010]. At this field-induced phase transition, pronounced changes in the magnetostriction appear. We simulated the element-resolved magnetization using a two-sublattice model and extracted the in-plane anisotropy constant. The present study shows the importance of microscopic soft x-ray dichroism experiments in the pulsed-field regime to study field-induced phase transitions that allow to determine fundamental magnetic parameters.

[1] R. Skomski and J. M. D. Coey, Permanent Magnetism (CRC Press, 1999).

[2] N. H. Duc, in Handbook on the Physics and Chemistry of Rare Earths, Vol. 24, edited by K. A. Gschneidner (Elsevier, Amsterdam, 1997), p. 339.

[3] J. J. M. Franse and R. J. Radwański, in Handbook of Magnetic Materials, Vol. 7, edited by K. H. J. Buschow (Elsevier, Amsterdam, 1993), p. 307.

[4] R. Ballou, B. Gorges, R. Lemaire, H. Rakoto, and J. C. Ousset, Field induced transition from collinear to canted magnetic structures in TbCo$_5$, Physica B **155**, 266 (1989).

[5] J. J. M. Franse, F. E. Kayzel, and N. P. Thuy, Exchange and anisotropy in 3d-4f compounds, J. Magn. Magn. Mater. **129**, 26 (1994).

[6] H. Kato, D. W. Lim, M. Yamada, Y. Nakagawa, H. A. Katori, and T. Goto, Field-induced phase transitions in ferrimagnetic R2Fe14B in ultra-high magnetic fields, Physica B, **211**, 105 (1995).

[7] A. V. Andreev, M. D. Kuz'Min, Y. Narumi, Y. Skourski, N. V. Kudrevatykh, K. Kindo, F. R. de Boer, and J. Wosnitza, High-field magnetization study of a Tm_2Co_{17} single crystal, Phys. Rev. B **81**, 134429 (2010).

[8] O. Isnard, A. V. Andreev, M. D. Kuz'min, Y. Skourski, D. I. Gorbunov, J. Wosnitza, N. V. Kudrevatykh, A. Iwasa, A. Kondo, A. Matsuo *et al.*, High magnetic field study of the Tm_2Fe_{17} and $Tm_2Fe_{17}D_{3.2}$ compounds, Phys. Rev. B **88**, 174406 (2013).

[9] D. P. Kozlenko, E. Burzo, P. Vlaic, S. E. Kichanov, A. V. Rutkauskas, and B. N. Savenko, Sequential cobalt magnetization collapse in $ErCo_2$: beyond the limits of itinerant electron metamagnetism, Sci. Rep. **5**, 8620 (2015).

[10] A. K. Zvezdin, in: K. H. J. Buschow (Ed.), Handbook of Magnetic Materials, vol. 9, Elsevier, Amsterdam, p. 405 (1995).

[11] A. Sarkis, and E. Callen, Magnetic anisotropy of rare-earth-transition-metal compounds, Phys. Rev. B **26**, 3870 (1982).

[12] D. I. Gorbunov, S. Yasin, A. V. Andreev, Y. Skourski, N. V. Mushnikov, E. V. Rosenfeld, S. Zherlitsyn, and J. Wosnitza, Magnetic anisotropy and magnetic phase transitions in RFe_5Al_7, J. Magn. Magn. Mater. **383**, 208 (2015).

[13] W. Suski, in Handbook on the Physics and Chemistry of Rare Earths, edited by K. A. Gschneidner, Jr. and L. Eyring (Elsevier, Amsterdam, 1996), Vol. 22, p. 143.

[14] D. I. Gorbunov, A. V. Andreev, S. Daniš, and J. Pospíšil, Evolution of magnetism in $LuFe_xAl_{12-x}$ (4 ≤ x ≤ 6) single crystals, J. Alloys Compd. **563**, 63 (2013).

[15] D. I. Gorbunov, S. Yasin, A. V. Andreev, Y. Skourski, S. Zherlitsyn, and J. Wosnitza, Magnetization and magnetoacoustics of single-crystalline $ErFe_5Al_7$ in high magnetic fields, J. Magn. Magn. Mater. **357**, 61 (2014).

[16] D. I. Gorbunov, S. Yasin, A. V. Andreev, N. V. Mushnikov, Y. Skourski, S. Zherlitsyn, and J. Wosnitza, Spontaneous and field-induced phase transitions in $TbFe_5Al_7$, J. Magn. Magn. Mater. **365**, 56 (2014).

[17] Sh. Yamamoto, D. I. Gorbunov, H. Akai, H. Yasumura, Y. Kotani, T. Nakamura, T. Kato, N. V. Mushnikov, A. V. Andreev, H. Nojiri, and J. Wosnitza, Element- and orbital-selective magnetic coherent rotation at the first-order phase transition of a hard uniaxial ferrimagnet, Phys. Rev. B **101**, 174430 (2020).

[18] D. I. Gorbunov, S. Yasin, A. V. Andreev, N. V. Mushnikov, E. V. Rosenfeld, Y. Skourski, S. Zherlitsyn, and J. Wosnitza, Phase transitions of anisotropic and exchange origins in $TmFe_5Al_7$, Phys. Rev. B **89**, 214417 (2014).

[19] D. I. Gorbunov, C. Strohm, M. S. Henriques, P. van der Linden, B. Pedersen, N. V. Mushnikov, E. V. Rosenfeld, V. Petříček, O. Mathon, J. Wosnitza, and A. V. Andreev, Microscopic Nature of the First-Order Field-Induced Phase Transition in the Strongly Anisotropic Ferrimagnet $HoFe_5Al_7$, Phys. Rev. Lett. **122**, 127205 (2019).

[20] M. A. Laguna-Marco, J. Chaboy, and H. Maruyama, Element-selective thermal x-ray magnetic circular dichroism study through the magnetic compensation temperature of Ho_6Fe_{23}, Phys. Rev. B **72**, 094408 (2005).

[21] J. Chaboy, M. A. Laguna-Marco, M. C. Sánchez, H. Maruyama, N. Kawamura, and M. Suzuki, Rare-earth orbital contribution to the Fe K-edge x-ray magnetic circular dichroism in rare-earth transition-metal intermetallic compounds, Phys. Rev. B **69**, 134421 (2004).

[22] D. I. Gorbunov and A. V. Andreev, Magnetic properties of single-crystalline $TbFe_5Al_7$, J. Alloys Compd. **577**, 203 (2013).

[23] Y. Skourski, M. D. Kuz'min, K. P. Skokov, A. V. Andreev, and J. Wosnitza, High-field magnetization of Ho_2Fe_{17}, Phys. Rev. B **83**, 214420 (2011).

[24] R. Daou, F. Weickert, M. Nicklas, F. Steglich, A. Haase, and M. Doerr, High resolution magnetostriction measurements in pulsed magnetic fields using fiber Bragg gratings, Rev. Sci. Instrum. **81**, 033909 (2010).

[25] Y. Senba, H. Ohashi, Y. Kotani, T. Nakamura, T. Muro, T. Ohkochi, N. Tsuji, H. Kishimoto, T. Miura, M. Tanaka *et al.*, Upgrade of beamline BL25SU for soft x-ray imaging and spectroscopy of solid using nano-and micro-focused beams at SPring-8, AIP Conf. Proc. **1741**, 030044 (2016).

[26] T. Hirono, H. Kimura, T. Muro, Y. Saitoh, and T. Ishikawa, Full polarization measurement of SR emitted from twin helical undulators with use of Sc/Cr multilayers at near 400 eV, J. Electron Spectros. Relat. Phenomena **144**, 1097 (2005).

[27] T. Nakamura, Y. Narumi, T. Hirono, M. Hayashi, K. Kodama, M. Tsunoda, S. Isogami, H. Takahashi, T. Kinoshita, K. Kindo *et al.*, Soft X-ray magnetic circular dichroism of a CoFe/MnIr exchange bias film under pulsed high magnetic field, Appl. Phys. Express **4**, 066602 (2011).

[28] W. Kockelmann, W. Schäfer, G. Will, P. Fischer, and J. Gal, Neutron diffraction study of the ferrimagnetic structures of RFe_5Al_7 compounds with R= Tb, Dy, Ho, Er, Tm, J. Alloys Compd. **207**, 311 (1994).

[29] D. Gignoux and D. Schmitt, in Handbook of Magnetic Materials, edited by K. H. J. Buschow, Vol. 10 (Elsevier, Amsterdam, 1997), p. 239.

[30] I. Felner and I. Nowik, Spin glass phenomena in $TbFe_xAl_{12-x}$, J. Magn. Magn. Mater. **74**, 31 (1988).

[31] N. Y. Schmidt, S. Laureti, F. Radu, H. Ryll, C. Luo, F. d'Acapito, S. Tripathi, E. Goering, E. Weller, and M. Albrecht, Structural and magnetic properties of FePt-Tb alloy thin films, Phys. Rev. B **100**, 064428 (2019).

[32] C. T. Chen, Y. U. Idzerda, H-J. Lin, N. V. Smith, G. Meigs, E. Chaban, G. H. Ho, E. Pellegrin, and F. Sette, Experimental confirmation of the X-ray magnetic circular dichroism sum rules for iron and cobalt, Phys. Rev. Lett. **75**, 152 (1995).

[33] G. van der Laan, B. T. Thole, G. A. Sawatzky, J. B. Goedkoop, J. C. Fuggle, J. -M. Esteva, R. Karnatak, J. P. Remeika, and H. A. Dabkowska, Experimental proof of magnetic x-ray dichroism, Phys. Rev. B **34**, 6529 (1986).

[34] J. Vogel, M. Sacchi, R. J. H. Kappert, J. C. Fuggle, J. B. Goedkoop, N. B. Brookes, G. van der Laan,

and E. E. Marinero, Magnetic properties of Fe and Tb in Tb_xFe_{1-x} amorphous films studied with soft x-ray circular and linear dichroism, J. Magn. Magn. Mater. **150**, 293 (1995).

[35] M. M. Schwickert, G. Y. Guo, M. A. Tomaz, W. L. O'Brien, and G. R. Harp, X-ray magnetic linear dichroism in absorption at the L edge of metallic Co,

Fe, Cr, and V, Phys. Rev. B **58**, R4289 (1998).

[36] K. Chen, D. Lott, F. Radu, F. Choueikani, E. Otero, and P. Ohresser, Temperature-dependent magnetic properties of ferrimagnetic $DyCo_3$ alloy films, Phys. Rev. B **91**, 024409 (2015).